Efficient Photoinduced Charge Separation in a BODIPY−C60 Dyad

Efficient Photoinduced Charge Separation in a BODIPY–C_{60} Dyad

Alessandro Iagatti,[†,‡,§] Lorenzo Cupellini,[§,∥] Giacomo Biagiotti,[⊥] Stefano Caprasecca,[∥] Stefano Fedeli,[⊥] Andrea Lapini,[†,‡] Eleonora Ussano,[#] Stefano Cicchi,[⊥] Paolo Foggi,[†,‡,¶] Massimo Marcaccio,[#] Benedetta Mennucci,[∥] and Mariangela Di Donato*[,†,‡,⊥]

[†]LENS (European Laboratory for Nonlinear Spectroscopy), via N. Carrara 1, 50019 Sesto Fiorentino, Italy

[‡]INO-CNR (Istituto Nazionale di Ottica), Largo Fermi 6, 50125 Firenze, Italy

[∥]Dipartimento di Chimica e Chimica Industriale, Università di Pisa, via G. Moruzzi 13, 56124 Pisa, Italy

[⊥]Dipartimento di Chimica "Ugo Schiff", Università di Firenze, via della Lastruccia 13, 50019 Sesto Fiorentino, Italy

[#]Dipartimento di Chimica "G. Ciamician", Università di Bologna, via Selmi 2, 40126 Bologna, Italy

[¶]Dipartimento di Chimica, Università di Perugia, via Elce di Sotto 8, 06100 Perugia, Italy

Supporting Information

ABSTRACT: A donor–acceptor dyad composed of a BF_2-chelated dipyrromethene (BODIPY) and a C_{60} fullerene has been newly synthesized and characterized. The two moieties are linked by direct addition of an azido substituted BODIPY on the C_{60}, producing an imino–fullerene–BODIPY adduct. The photoinduced charge transfer process in this system was studied by ultrafast transient absorption spectroscopy. Electron transfer toward the fullerene was found to occur selectively exciting both the BODIPY chromophore at 475 nm and the C_{60} unit at 266 nm on a time scale of a few picoseconds, but the dynamics of charge separation was different in the two cases. Eletrochemical studies provided information on the redox potentials of the involved species and spectroelectrochemical measurements allowed to unambiguously assign the absorption band of the oxidized BODIPY moiety, which helped in the interpretation of the transient absorption spectra. The experimental studies were complemented by a theoretical analysis based on DFT computations of the excited state energies of the two components and their electronic couplings, which allowed identification of the charge transfer mechanism and rationalization of the different kinetic behavior observed by changing the excitation conditions.

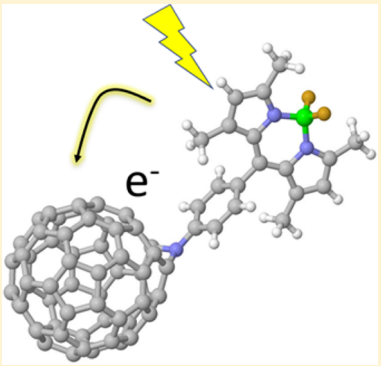

1. INTRODUCTION

The efficiency of natural photosynthetic complexes in harvesting solar light and transform it into useful chemical energy has promoted many efforts to mimic this process by developing artificial systems. Photosynthetic energy conversion is initiated by light absorption from an antenna system, composed by a number of chromophores that transfer energy to a reaction center in a very fast and efficient way. Here a series of electron transfer processes occur, finally generating a long-lived charge separated state.

In recent years significant synthetic effort has been devoted to produce both artificial antennas and electron donor–acceptor units.[1−7] In developing electron transfer adducts, the choice of the acceptor has been often directed toward fullerenes, since the presence of many closely spaced electronic levels, the high degree of charge delocalization within an extended π-conjugated structure, and the small reorganization energies make these molecules an ideal system to act as electron acceptor in a charge separated state. Different natural based chromophores have been used as electron donors, such as phorphyrins and phthalocyanines, however the choice has not been limited to these classes of systems.[8−13] Recently, among the commonly used artificial photosynthetic chromophores, BF_2-chelated dipyrromethene compounds, usually indicated as BODIPY, have attracted notable attention and have been used both as building blocks of antenna systems and as charge separating units.[8,14−20] BODIPY are interesting dyes, because of both their high chemical stability and their convenient electronic properties, such as high absorption coefficients and emission quantum yields. Another remarkable aspect connected to their use in artificial photosynthetic devices is the possibility of easily tuning their spectral properties, by introducing and/or varying one or more substituents in positions 1–7 and 3–5 (Scheme 1).[21,22] This valuable tunability makes the BODIPY dyes very versatile, opening the possibility of extending the absorption cross section of an artificial device over a wide spectral range.

Taking advantage of all these properties, recently a high number of BODIPY–fullerene donor–acceptor systems, capable of performing fast charge separation and relatively slow charge recombination, have been synthesized and characterized.[8,14,17,19] Furthermore, in a number of studies

Scheme 1. Structures of the Analyzed Compounds

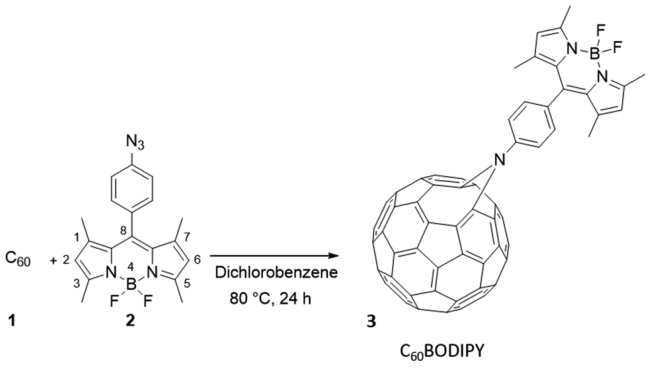

the effect of solvent, temperature, and other external conditions on the efficiency of charge separation has been investigated, providing important information about the factors influencing the efficiency of the process.[2,3,7]

In this work we have synthesized and characterized a simple electron-donor−acceptor dyad based on a BODIPY−C_{60} complex. What makes our system different from most of the previously analyzed ones concerns the molecular bridge between donor and acceptor, which is here virtually absent, the two moieties being linked by direct addition of an azido substituted BODIPY[23] on the C_{60}, producing an imino−fullerene−BODIPY adduct.[24−26] By exploiting the synthetic unicity of our approach we aimed at investigating whether such a system would act as a dyad, thus preserving the molecular identity of the two connected molecules, with localized molecular orbitals, or a more extended delocalization of electron density would occur. The excited state evolution of the system was investigated by ultrafast transient absorption spectroscopy. We found that upon selective excitation of both moieties electron transfer toward the C_{60} occurred on a time scale of a few picoseconds, although with a different kinetics in the two cases. We furthermore characterized the system through electrochemical studies, which provided information on the redox potentials of the involved species. Also, spectroelectrochemical measurements were performed, which allowed unambiguous assignment of the absorption band of the oxidized BODIPY moiety. The experimental studies were complemented by a thorough theoretical analysis based on DFT computations of the excited state energies of the two molecules composing the dyad. Furthermore, their electronic couplings were theoretically estimated, allowing the comparison of the computed and experimental electron transfer kinetic constants, as well as the rationalization of the observed wavelength excitation-dependent kinetic behavior, and hence the identification of the charge transfer mechanism.

2. EXPERIMENTAL DETAILS

2.1. Synthesis. A suspension of fullerene C_{60} (100 mg, 0.14 mmol) and BODIPY (51 mg, 1 equiv) in dichlorobenzene (mixture of isomers, 10 mL) was heated at 80 °C under stirring and N_2 atmosphere for 24 h (Scheme 1). The solution was then cooled to room temperature and diluted with 40 mL of CH_3CN. The suspension was left at 4 °C for 12 h and centrifuged at 3000*g* for 10 min. The solid precipitate was purified by flash column chromatography affording unreacted C_{60} (53 mg) and the single adduct **3** (16.5 mg, 24% yield calculated on the conversion of C_{60}). Nontrace amount of the eventual [6,6]-bridged aziridino fullerene derivative was isolated.

Compund **3**: ^{1}H NMR (CS_2/$CDCl_3$ 1:2, 400 MHz) δ 7.69 (AA′ part of an AA′BB′ system, 2H), 7.31 (BB′ part of an AA′BB′ system, 2H); 5.98 (s, 2H, pyrrole ring H), 2.53 (s, 6H, 2 × CH_3), 1.55 (s, 6H, 2 × CH_3) ppm; ^{13}C NMR (CS_2/$CDCl_3$ 1:2, 100 MHz) δ 155.4, 148.2, 147.5, 144.8, 144.7, 144.6, 144.4, 144.3, 144.2, 144.1, 144.0, 143.9, 143.8, 143.6, 143.5, 143.4, 143.3, 143.0, 142.9, 142.8, 141.8, 141.5, 141.04, 140.9, 140.0, 139.9, 139.8, 138.7, 138.3, 137.7, 137.2, 136.6, 134.8, 131.7, 129.11, 129.0, 121,4, 116.8, 14.9, 14.7 ppm; ESI mass (MeOH) (−) m/z = 1057.08

2.2. Transient Absorption Measurements. The apparatus used for the transient absorption spectroscopy (TAS) measurements has been described in detail in previous works.[27] A Ti:sapphire laser oscillator (Spectra Physics Tsunami) pumped by the second harmonic from a Nd:YVO (Spectra Physics Millennia) produced 70 fs pulses at 800 nm, which were stretched and amplified at 1 kHz repetition rate by a regenerative amplifier (BMI Alpha 1000). After compression a total average power of 450−500 mW and pulse duration of 100 fs are obtained. The repetition rate of the output beam was reduced to 100 Hz by a mechanical chopper in order to avoid the photodegradation of the sample. Excitation pulses at 475 nm have been obtained by mixing the output of an optical parametric generator and amplifier (OPG-OPA) based on a BBO crystal (TOPAS by Light Conversion, Vilnius, Lithuania) with the residual laser fundamental,[28,29] while pulses at 266 and 400 nm have been obtained respectively by third and second harmonic generation of the fundamental 800 nm laser output. At all excitation wavelengths the pump beam polarization has been set to magic angle with respect to the probe beam by rotating a $\lambda/2$ plate so as to exclude rotational contributions to the transient signal. The probe pulse was generated by focusing a small portion of the 800 nm radiation on a 3 mm thick CaF_2 window mounted on a motorized translation stage. The continuum light was optimized for the 350−750 nm wavelength range, and a moveable delay line made it possible to increase the time-of-arrival difference of the pump and probe beams up to 2.0 ns. Multichannel detection for transient spectroscopy was achieved by sending the white light continuum after passing through the sample to a flat field monochromator coupled to a homemade CCD detector [http://lens.unifi.it/ew]. TAS measurements were carried out in a static cell (2 mm thick) under magnetic stirring in order to refresh the solution and avoid photodegradation.

The visible absorption spectra were recorded using a PerkinElmer LAMBDA 950, while fluorescence was recorded using a PerkinElmer LS55 fluorimeter. The integrity of the sample was checked by recording its visible absorption spectrum before and after the time-resolved measurements. The OD of the sample at the excitation wavelength was between 0.2 and 0.5 in all the examined samples. Time resolved measurements were performed at room temperature in chloroform and benzonitrile. All the solutions were saturated with nitrogen, and the cuvettes used during the data acquisition were sealed before the measurement.

2.3. Electrochemistry and UV−Vis Spectroelectrochemistry. Tetrabutylammonium hexafluorophosphate (TBAH) was used as received as supporting electrolyte, and it was electrochemical or analytical grade from Sigma-Aldrich. Dry dichloromethane (DCM) was purified and dried as

previously reported,[30] stored in a specially designed Schlenk flask, and protected from light.

Shortly before the experiment was performed, the solvent was distilled via a closed system into an electrochemical cell containing the supporting electrolyte and the species under examination. Electrochemical experiments were carried out in an airtight single-compartment cell described elsewhere[31] by using platinum as working electrode, a platinum spiral as counter electrode, and a silver spiral as a quasi-reference electrode. The cell containing the supporting electrolyte and the electroactive compound was dried under vacuum at about 110 °C for at least 48 h before each experiment. All the $E_{1/2}$ potentials have been directly obtained from CV curves as averages of the cathodic and anodic peak potentials for one-electron peaks and by digital simulation for those processes closely spaced in multielectron voltammetric peaks. The $E_{1/2}$ values are referred to an aqueous saturated calomel electrode (SCE) and have been determined by adding, at the end of each experiment, ferrocene as an internal standard and measuring them with respect to either the ferrocenium/ferrocene or decamethylferrocenium/decamethylferrocene couple standard potential. The potentials thus obtained were not corrected for the two unknown contributions of the liquid junction potential between the organic phase and the aqueous SCE solution.

Voltammograms were recorded with an AMEL model 552 potentiostat or a custom-made fast potentiostat[31,32] controlled by an AMEL model 568 programmable function generator. The potentiostat was interfaced to a Nicolet model 3091 digital oscilloscope and the data transferred to a personal computer by the program Antigona.[33] Minimization of the uncompensated resistance effect in the voltammetric measurements was achieved by the positive-feedback circuit of the potentiostat. Digital simulations of the cyclic voltammetric curves were carried out either by Antigona or DigiSim 3.0.

The UV−vis−NIR spectroelectrochemical experiments were carried out using a quartz OTTLE cell with a 0.03 cm path length. Temperature control was achieved by a special homemade cell holder with quartz windows, in which two nitrogen fluxes (one at room temperature and the other at low temperature) are regulated by two needle valves. All the spectra were recorded by a Cary 5 spectrophotometer. All the experimental details for the spectroelectrochemical setup were reported elsewhere.[34,35]

2.4. Computational Details. The calculations were performed in a locally modified version of the Gaussian software. Geometry optimizations were carried out at the B3LYP/6-31G(d) level, while excited state calculations used the CAM-B3LYP functional and 6-31+G(d) basis set, within the Tamm−Dancoff approximation (TDA). The solvent was included at all levels by employing the polarizable continuum model (PCM) in its IEF-PCM formulation.[36] Within this model, the solvent is treated as a structureless continuum and characterized by its dielectric constant. The solvent polarization as a response to the presence of the solute is represented as a set of apparent charges placed on the molecular cavity surrounding the solute. Such charges act back on the solute by entering the molecular Hamiltonian and therefore polarizing the electron density. The effect of the solvent can be included on both ground and excited state calculations, and a recent extension has allowed to explicitly consider it in the electronic couplings.

In the following, we shall refer to the two fragments into which the system has been partitioned (BODIPY and $C_{60}NH$) as BODIPY and C_{60}, respectively.

2.4.1. Excitation Energy Transfer Rates. The excitation energy transfer (EET) rates have been computed assuming the Fermi golden rule:

$$k_{\mathrm{EET}} = \frac{2\pi}{\hbar} |V_{\mathrm{DA}}|^2 J$$

where V_{DA} is the electronic coupling and J is the spectral overlap. The former are computed using a well-established perturbative approach based on transition densities.[37] Two separate excited state calculations are carried out on the energy donor and acceptor, and the relative transition densities are used to compute the couplings:

$$V_{\mathrm{DA}} = \int \mathrm{d}\mathbf{r}\, \mathrm{d}\mathbf{r}'\, \tilde{\rho}_{\mathrm{D}}(\mathbf{r}) \frac{1}{|\mathbf{r} - \mathbf{r}'|} \tilde{\rho}_{\mathrm{A}}(\mathbf{r}') + \int \mathrm{d}\mathbf{r}\, \mathrm{d}\mathbf{r}'\, \tilde{\rho}_{\mathrm{D}}(\mathbf{r})\, g_{\mathrm{xc}} \tilde{\rho}_{\mathrm{A}}(\mathbf{r}') - \sum_t \left[\int \mathrm{d}\mathbf{r} \frac{\tilde{\rho}_{\mathrm{D}}}{|\mathbf{r} - \mathbf{r}_t|} \right] q_t(\epsilon_\infty | \tilde{\rho}_{\mathrm{A}})$$

where D and A label the two fragments, $\tilde{\rho}_{\mathrm{D}}$ and $\tilde{\rho}_{\mathrm{A}}$ are their transition densities, respectively, and the three terms on the right-hand side of the equation are Coulomb, exchange-correlation, and explicit solvent contributions to the coupling, respectively. The latter, in particular, is written in terms of the electrostatic interaction between the transition density of one fragment and the apparent polarization charges induced by the other fragment. The summation index t runs over the PCM charges. Note that these have been obtained using the optical dielectric constant of the solvent, ϵ_∞, instead of the static one, since only the electronic degrees of freedom of the environment molecules are fast enough to immediately respond to the electronic excitation process, while the polarization response associated with the nuclear reorganization is in a state of nonequilibrium.

As most of the initial states are optically dark and overlapping, there is no easy way to compute the spectral overlap J. However, it has been estimated by placing Gaussian functions, with a fwhm of 500 cm^{-1}, centered at the excitation energies, and then computing analytically their overlap. This procedure is useful to identify the states with non-negligible overlap, but we remind that it only returns qualitative results, and should not be assumed quantitative.

2.4.2. Electron and Hole Transfer Rates. The rates for electron and hole transfers (ET and HT, respectively) have been calculated assuming a Fermi golden rule as for EET, employing Marcus theory:

$$k_{\mathrm{Marcus}} = \frac{2\pi}{\hbar} |V_{\mathrm{DA}}|^2 \frac{1}{\sqrt{4\pi\lambda k_{\mathrm{b}} T}} \exp\left[-\frac{(\lambda + \Delta G^\circ)^2}{4\lambda k_{\mathrm{b}} T} \right]$$

where V_{DA} is the electronic coupling, k_{b} the Boltzmann constant, T the temperature, ΔG° the free energy of reaction, and λ the reorganization energy.

The calculation of the electronic couplings involved in ET and HT cannot be performed using the fragment-based transition density approach outlined before, since both a localized and charge transfer (CT) state are involved, and the latter has contributions from the molecular orbitals of both fragments. An alternative procedure based on the fragment charge difference (FCD) model of Voityuk[38] has been carried out instead: an electronic structure calculation is first performed on the whole bichromophoric system, and the resulting

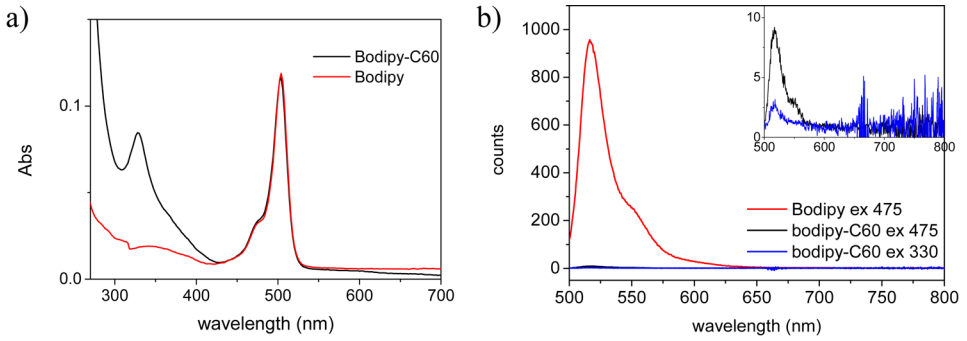

Figure 1. (a) Absorption spectrum of the BODIPY–C_{60} dyad in chloroform (black line) and the isolated BODIPY moiety (red line). (b) Fluorescence spectra of the isolated BODIPY (red line, excitation 475 nm) and the BODIPY–C_{60} dyad excited at 475 nm (black line) and 330 nm (blue line). The intensity of the dyad fluorescence is better visualized in the inset.

adiabatic electronic states obtained. The initial and final diabatic states are defined as those where the charge is maximally localized on either the donor or the acceptor. The off-diagonal element of the Hamiltonian in the diabatic basis is the electronic coupling V_{DA}. The reorganization energy λ of the electron transfer reaction

$$D^* + A \rightarrow D^+ + A^-$$

has been estimated as the average of backward and forward reorganization energies (λ_{bw} and λ_{fw}, respectively), following the procedure described in Lee et al.:[39]

$$\lambda_{bw} = E(D^*@D^+) - E(D^*@D^*) + E(A@A^-) - E(A@A)$$
$$= \lambda_{bw,D} + \lambda_{bw,A}$$

$$\lambda_{fw} = E(D^+@D^*) - E(D^+@D^+) + E(A^-@A) - E(A^-@A^-)$$
$$= \lambda_{fw,D} + \lambda_{fw,A}$$

where the notation $E(F@F')$ indicates that the energy is calculated for fragment F at its F′ geometry. The total reorganization energy is computed as

$$\lambda = \lambda_D + \lambda_A = [(\lambda_{bw,D} + \lambda_{fw,D}) + (\lambda_{bw,A} + \lambda_{fw,A})]/2$$

When the calculation is performed in vacuo, λ corresponds to the inner sphere reorganization energy. The solvent relaxation, contributing to the outer sphere reorganization energy, can be obtained by performing the calculations in the presence of the solvent, with the correct equilibrium scheme.[40]

The free energy for electron transfer can also be estimated from the experimental redox potentials and donor excitation energy, using the Rehm–Weller approach,[41] according to the following equations:

$$-\Delta G_{ETCS} = E_{0-0} - (-\Delta G_{CR})$$

$$-\Delta G_{CR} = e(E_{ox} - E_{red}) + \Delta G_S + \Delta G_B$$

Here E_{0-0} is the energy of the lower excited state of the electron donor (2.48 eV in case of BODIPY), e is the electron charge, and E_{ox} and E_{red} are respectively the first oxidation potential of the donor and the first reduction potential of the acceptor. ΔG_S is the difference in solvation energies by passing from the reference solvent (DCM) to chloroform, and ΔG_B is the binding energy of between the positively charged donor and the negatively charged acceptor. Usually, ΔG_S and ΔG_B are estimated from the Rehm–Weller equation, assuming that D and A are well separated and spherical molecules. In our case, we used a more physical approach, estimating ΔG_S and ΔG_B from ab initio calculations: we computed E_{ox} and E_{red} in both DCM and chloroform, and obtained ΔG_S as

$$\Delta G_S = e(E_{ox,CHCl3} - E_{red,CHCl3}) - e(E_{ox,DCM} - E_{red,DCM})$$

Finally, the binding energy ΔG_B between the two oppositely charged fragments was calculated as the electrostatic interaction between atomic charges of D and A, scaled by the static dielectric constant of $CHCl_3$ ε_{CHCl_3}, to account for the solvent screening.

3. RESULTS AND DISCUSSION

3.1. Absorption and Fluorescence Measurements. The visible absorption spectrum of the BODIPY–C_{60} system is reported in Figure 1a and compared with the absorption spectrum of the isolated BODIPY fragment. It can be noticed that coordination with the C_{60} unit does not influence the absorption properties of the BODIPY, which always shows an absorption band centered at 500 nm. In the spectrum of the dyad an additional sharp band at 330 nm is observed, due to the fullerene molecule. Fluorescence of the BODIPY (Figure 1b), observed at 516 nm for the isolated molecule, is almost completely quenched in the dyad, suggesting the occurrence of excited state interactions between the two moieties. The concentration of the solutions of the isolated BODIPY and the dyad used for the fluorescence measurement have been adjusted in a way to have the same absorbance at 500 nm. It is evident that in the presence of the fullerene, the emission of the BODIPY unit is quenched by >90%. In principle fluorescence quenching could be due either to excitation energy transfer or to electron/hole transfer in the dyad. Excitation of the C_{60} band centered at 330 nm also does not induce BODIPY fluorescence, suggesting that excited state energy transfer from C_{60} to BODIPY is not the main reason for the observed emission quenching.

3.2. Electrochemistry and UV–Vis–NIR Spectroelectrochemistry. The electrochemical behavior of the dyad BODIPY–C_{60} in dichloromethane at room temperature is shown in Figure 2. On the negative potential side three reduction processes can be observed whereas on the positive one two oxidations occur (Table 1). Two out of three reductions are completely reversible one-electron processes, and by comparison with the voltammetric studies of pristine fullerene[42] they can confidently be attributed to the C_{60} moiety. The third voltammetric wave is completely irreversible, at a sweep rate of 1 V/s, and it is complicated by the presence of a small peak at higher negative potential. This is certainly due to

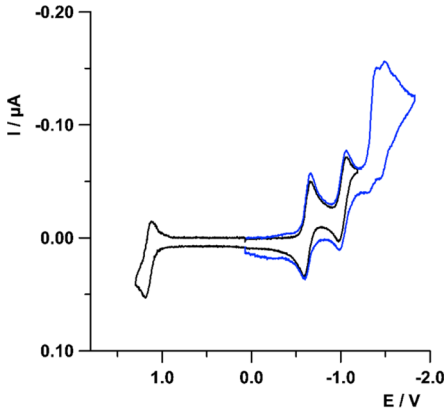

Figure 2. Cyclic voltammetric curves of species BODIPY−C_{60} 0.6 mM in 0.08 M TBAH/DCM solution. Sweep rate 1 V/s, working electrode Pt (125 μm, diameter), T = 25 °C.

Table 1. Half-Wave ($E_{1/2}$) Redox Potentials[a] (vs SCE) of All Compounds at 25 °C

	$E_{1/2}$/V				
	ox.		red.		
species	I	II	I	II	III
BODIPY−C_{60}	1.16	1.55	−0.63	−1.02	−1.38[b] −1.49[b]
BODIPY−Ph	1.14		−1.30	−2.26[b]	
C_{60}[c]	1.69	2.16	−0.64	−1.04	−1.47

[a]In a 0.08 M $TBAPF_6$/DCM solution. Working electrode: Pt disk (diameter: 125 μm) [b]Irreversible process; peak potential. [c]From ref 30: pristine C_{60} 0.15 mM in a 0.08 M $TBAAsF_6$/DCM solution.

a chemical reaction following up the electron transfer, with the product undergoing a further electron transfer process, i.e., an ECE mechanism that has not been further investigated in this work. Such a third reduction can involve part of the fullerene cage and in particular the aza-cyclopropane bridge, and it can be responsible for the observed irreversibility. Indeed DFT computations show that in the LUMO+2 orbital an antibonding contribution on the C_{60}−aza bridge is present (see Figure S.4).

As concerns the oxidation processes, the first process is reversible at 1 V/s while the second one has some degree of chemical irreversibility. The first voltammetric peak, at about +1.2 V, can be assigned to the BODIPY moiety as the potential is very close to the oxidation of both phenyl-BODIPY (BODIPY−Ph) and *p*-azidophenyl-BODIPY (BODIPY−N_3) in DCM (*vide infra*). The second oxidation, at +1.55 V, has a redox value compatible with that of the first oxidation of C_{60}.

As further electrochemical characterization, also aimed at attributing the main localization of the redox processes of the dyad BODIPY−C_{60}, voltammetric investigation of the BODIPY moiety has been carried out. Both BODIPY−N_3 and BODIPY−Ph have been studied under the same conditions of the dyad, and the results are reported in Figure S.2 and Figure S.3. BODIPY−N_3 shows two one-electron processes, a reversible oxidation at about +1.2 V and a chemically irreversible reduction with a peak potential at −1.3 V (Figure S.2a), whereas the species BODIPY−Ph allowed observation of one reduction more within the useful potential window (Figure S.2b). As concerns BODIPY−N_3, the irreversibility of the reduction at room temperature turns to disappear both increasing the sweep rate (complete reversibility at 100 V/s) and lowering the temperature (−60 °C; Figure S.3). The reactivity of the reduced BODIPY derivative can be attributed to the azide group, as also confirmed by the comparison with the voltammetric curves of BODIPY−Ph. In fact, for the latter compound the reduction occurs at the same potential but it is completely reversible. Moreover, extending the scan toward more negative potentials, BODIPY−Ph undergoes a second reduction which is completely irreversible even at higher scan rates.

It is worth noticing that the comparison of the redox potentials, for the oxidation and reduction processes, of BODIPY−C_{60} and BODIPY−Ph allows the main localization of the processes to be attributed. Thus, the first oxidation of the dyad is centered on the BODIPY moiety and the first two reductions are fullerene-centered whereas the third irreversible reduction is very close to the reduction of the BODIPY−Ph unit. The only difference is in the irreversibility, which can be associated with the reactivity of the aza-three-atom ring on the fullerene cage.

The measured half-wave redox potentials for all the considered species are reported in Table 1.

In order to ascertain the nature of the charge separated state of the dyad a UV−vis−NIR spectroelectrochemical investigation was performed in dichloromethane for both the BODIPY−C_{60} and the BODIPY moieties. In Figure 3 the

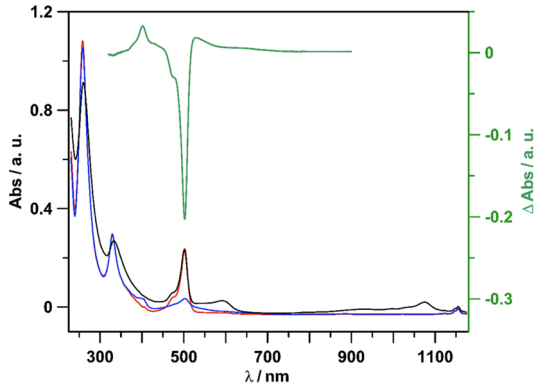

Figure 3. UV−vis−NIR spectra of the compound BODIPY−C_{60} 0.3 mM in 0.07 M TBAH/DCM solution; working electrode, Pt gauze; temperature = 0 °C. Spectra of the pristine compound (red trace), one-electron-oxidized species (blue trace), and one-electron reduced species (black trace). Difference spectrum of the oxidized state (green trace; pristine compound spectrum subtracted).

spectra of the three redox states of the dyad BODIPY−C_{60} have been plotted, together with the difference spectrum of the oxidized dyad. As reported above, the absorption spectrum of the BODIPY−C_{60} is made of bands attributable to fullerene (at about 260 and 330 nm) and to BODIPY, at about 500 nm. Upon exhaustive reduction of the dyad at −0.7 V, in the thin layer cavity of the spectroelectrochemical cell, it is possible to note a characteristic decrease and red shift of the two bands centered at about 260 and 330 nm. The final spectrum (black trace in Figure 3) is practically identical to that typically observed for the one-electron reduced pristine fullerene, C_{60}^-,[43] It is also noteworthy to highlight the growth of the typical bands in the NIR region, centered at 1000 nm. At opposite, when the dyad is oxidized, the spectrum is affected only at wavelengths relative to the absorption of the BODIPY moiety,

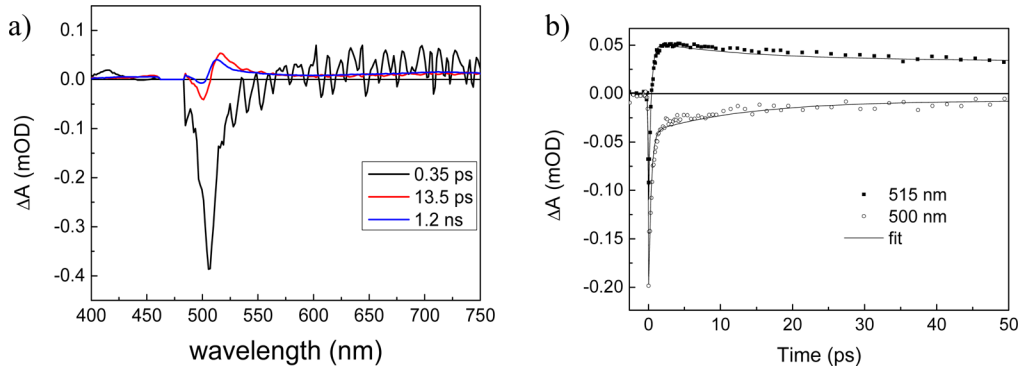

Figure 4. (a) EADS obtained by global analysis of the BODIPY−C_{60} transient spectra registered with 475 nm excitation. (b) Kinetic traces at 500 and 515 nm (scattered points) together with the fit obtained by global analysis.

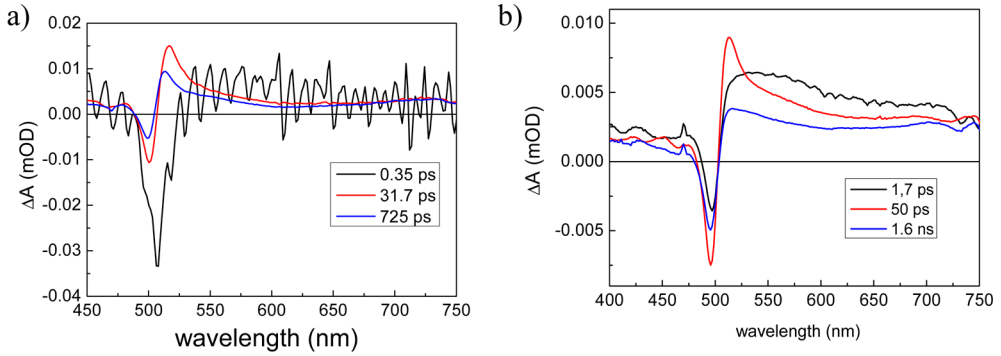

Figure 5. EADS obtained by global analysis of the BODIPY−C_{60} transient spectra registered with (a) 400 nm excitation and (b) 266 nm excitation.

thus showing a large decrease in the band at about 500 nm, which nearly disappears (blue trace). All these facts confirm the main localization of the redox processes reported above on the basis of voltammetric data.

The difference spectrum of the oxidized dyad, obtained by subtracting the spectrum of pristine BODIPY−C_{60}, in the visible region, accounts only for the variations attributable to the oxidation of BODIPY. As a matter of fact, it shows a sharp decrease at about 500 nm, with the growth of two minor bands at immediately shorter and longer wavelengths (green trace in Figure 3).

It is important to point out that the differential spectrum thus obtained is perfectly in line with the transient spectrum gathered by photoexcitation (see infra).

3.3. Time Resolved Spectroscopy. Transient absorption measurements have been repeated, exciting the sample at three different wavelengths: 475 nm, mostly exciting the BODIPY unit; 400 nm, where both chromophores have comparable absorbance; and 266 nm, mostly exciting the fullerene unit. The transient data have been analyzed by simultaneously fitting all the kinetic traces with exponential decay functions (global analysis). Three kinetic components were necessary in all cases to satisfactorily fit the data. Figure 4 reports the associated spectral components (EADS, evolution associated decay spectra) and the kinetic traces at 500 and 515 nm, together with the fit obtained from global analysis for transient data recorded upon excitation at 475 nm.

Excitation of the sample on the BODIPY unit at 475 nm induces the immediate appearance of an intense negative band in the time-resolved spectra, peaked at 505 nm. This band, which can be attributed to the bleaching of the BODIPY visible absorption and its stimulated emission, recovers by almost 90% in 0.35 ps. In the subsequent spectral record (red line in Figure 4a) a small differential signal at 501(−)/517(+) nm is observed. On the basis of the spectroelectrochemistry measurements, showing that upon oxidation of the dyad the BODIPY absorption at ca. 500 nm greatly reduces in intensity and slightly red shifts, we attribute the positive band at 517 nm to the $BODIPY^+$ species, thus indicating the occurrence of ultrafast electron transfer in the BODIPY−C_{60} adduct. In the successive evolution, the negative signal at 501 nm further decays, while the positive band at 517 nm blue shifts by 3 nm. This evolution can be interpreted in terms of vibrational cooling, and relaxation of the charge separated state. The transient signal completely recovers within 1.2 ns, as estimated by global analysis. Experiments at this excitation wavelength have been repeated in benzonitrile with very similar results, showing the occurrence of charge separation on a sub-picosecond time scale. The only difference is on a relatively higher signal decay on a ca. 45 ps time scale, indicating that in this case at least 50% of charge recombination occurs on this time scale. The EADS obtained from global analysis and selected time traces for measurements in benzonitrile are reported in the Supporting Information.

Figure 5 reports the EADS obtained applying a similar global analysis procedure to the transient data registered by exciting the sample at 400 and 266 nm.

In Figure 5 it can be noticed that the differential signal at 501(−)/517(+) nm is observed in the transient spectra also when different excitations are employed, but the time evolution of the signal is different in these cases. When the less selective 400 nm excitation is employed, again the immediate appearance of the BODIPY bleaching is observed, together with a small broad absorption extending over the 500−700 nm spectral

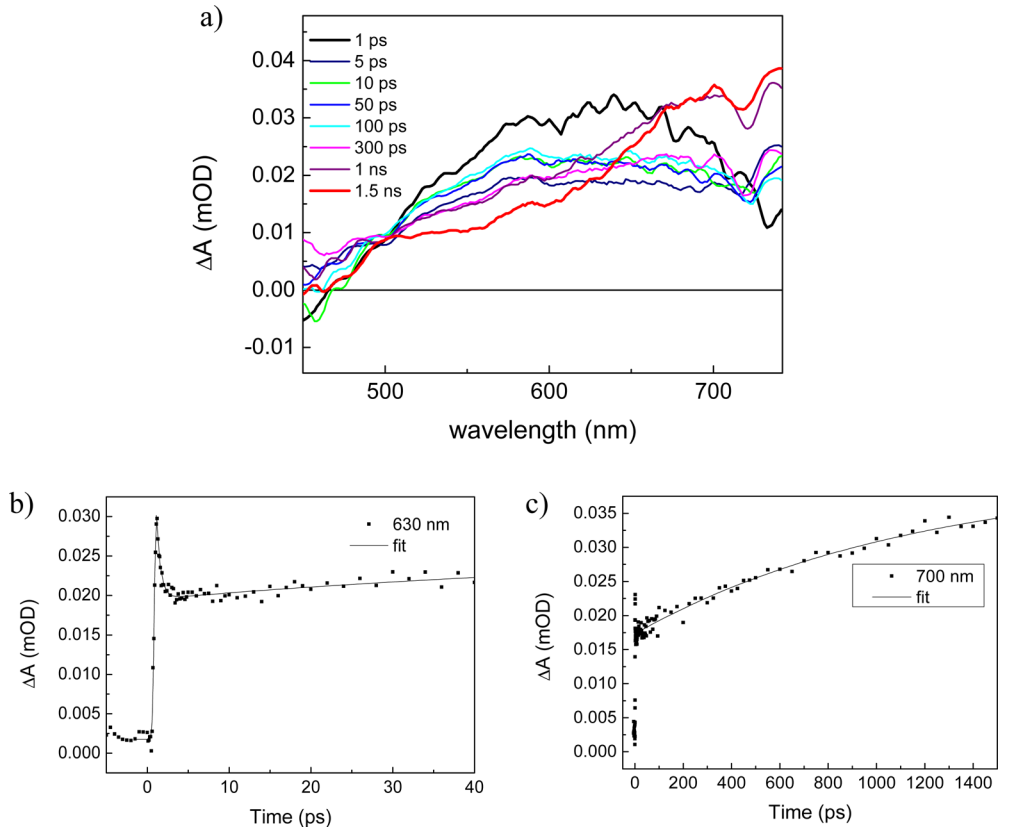

Figure 6. (a) Transient absorption spectra of C_{60} in toluene solution upon 400 nm excitation at selected pump−probe delay. (b) Kinetic trace at 630 nm (scattered points) and fit (solid line) obtained with a three exponential function with time constants $\tau 1$ = 500 fs, $\tau 2$ = 80 ps, $\tau 3$ = 1.2 ns. (c) Kinetic trace at 700 nm (scattered points) and fit (solid line) with a single exponential rise function with time constant τ = 1.2 ns. Early time points (t < 2 ps) are excluded from the fit at this wavelength.

range. The BODIPY bleaching partially recovers with the same kinetics observed in the case of 475 nm excitation (lifetime 0.35 ps), and the time-resolved spectra evolve giving rise to the appearance of the same differential signal already observed in the previous case, attributed to the formation of the $BODIPY^{+}$. The following evolution is again similar to what was previously observed, although occurring with a slower time constant (lifetime 31.7 ps). The transient signals completely recover in less than 1 ns. At 266 nm excitation most of the pump is absorbed by the C_{60} moiety, whose extinction coefficient at this wavelength is higher than that of BODIPY. Nevertheless, the immediate appearance of a small signal attributable to the BODIPY bleaching is observed also in this case, which can be due to partial direct excitation of this molecule, also at this wavelength, or to the occurrence of ultrafast energy and/or electron exchange between the two moieties of the dyad. Besides the BODIPY bleaching, a broad absorption extending over more than 200 nm is observed at short time delays, which can be attributed to excited state absorption of the fullerene molecule (*vide infra*).[44,45]The broad absorption partially decays in 1.7 ps. At the same time the BODIPY negative band increases in intensity and the $BODIPY^{+}$ absorption band peaking at 515 nm develops. The signal decays biexponentially with a shorter lifetime of 45 ps and a longer one of 1.7 ns. The residual absorption signal in the redmost part of the spectrum could account for the formation of the fullerene triplet state, which has a distinctive peak in this region. However, considering the signal intensity we shall conclude that the yield of triplet formation in the dyad is certainly lower than that observed for the pristine fullerene in solution.

In order to better evaluate the ultrafast relaxation processes occurring when exciting the C_{60} moiety, transient absorption spectra of C_{60} dissolved in deaerated toluene were also recorded, employing an excitation wavelength of 400 nm. The time-resolved spectra and the kinetic evolution retrieved from the analysis of the measured time traces, reported in Figure 6, are in line with previously reported data (see the Supporting Information for discussion).[44−48]

3.4. Computational Results. The experimental results indicate the occurrence of photoinduced electron transfer from BODIPY toward C_{60}, upon selective excitation of both molecules. The kinetics of charge separation is however different in the two cases. In order to elucidate the electron transfer mechanism operating at different excitations, we performed a theoretical analysis aimed at evaluating the electron transfer kinetic constant upon selective BODIPY excitation. In the case of C_{60} selective excitation two electron transfer pathways are in principle possible: (1) energy transfer toward BODIPY followed by electron transfer and (2) hole transfer from C_{60} to BODIPY. These two mechanisms have been theoretically compared by the estimation of the relative time constants. The possible excited state deactivation pathways are sketched in Scheme 2.

The calculated states have been assigned on the basis of their symmetry and comparison of our experimental and theoretical data with those reported in the literature.[48,49] On average, the

Scheme 2. 4-Orbital Models of the Electronic Processes Studied[a]

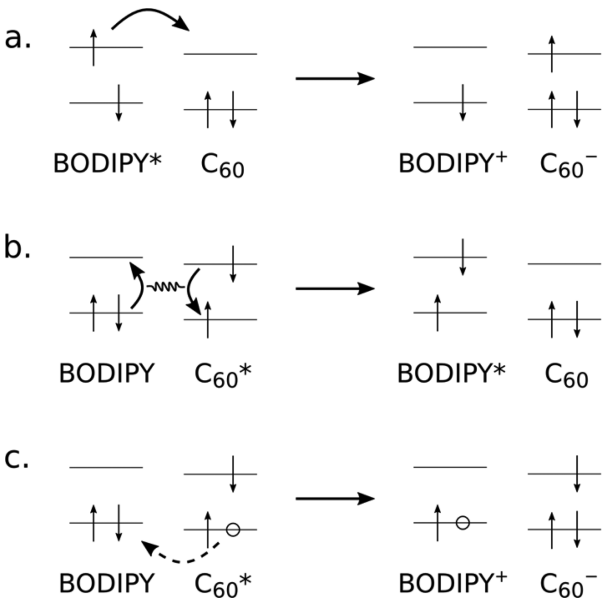

[a](a) Electron transfer (ET) from the excited BODIPY to the C_{60} moiety; (b) electronic energy transfer from the excited C_{60} to the BODIPY moiety; (c) electron transfer from the BODIPY to the excited C_{60} moieties, which is interpreted as a hole transfer (HT) from the excited C_{60} to the BODIPY.

excitation energies of C_{60} are overestimated by 0.6−0.7 eV, with a higher overestimation for the higher lying states.

The symmetry breaking due to the functionalization of the C_{60} allows the mixing of the states of different symmetry, particularly the lowest states, which are almost degenerate.

3.4.1. Electron Transfer from BODIPY to C_{60}. The electron transfer process from the excited BODIPY moiety to the C_{60} one can be schematically written as

$$\text{BODIPY*}\ C_{60} \rightarrow \text{BODIPY}^{+}\ C_{60}^{-}$$

The electronic coupling is calculated between the first adiabatic state localized on BODIPY and the BODIPY → C_{60} charge transfer states, which can be assigned by inspecting the natural transition orbitals (NTOs[49]). The HOMO and LUMO NTOs are shown in Figure 7. Panel a shows one of the charge transfer states, whose HOMO is localized on the BODIPY moiety and the LUMO on the C_{60} one. Panel b shows the HOMO and LUMO NTOs of the first BODIPY-centered state. The HOMOs of the two states practically coincide.

The effective electronic coupling calculated with the FCD method is 99.6 cm^{-1}. The reorganization energy λ was estimated as the average of backward and forward reorganization energies, as detailed above, where D = BODIPY and A = C_{60}. The inner sphere and total reorganization energies are reported in Table S.1.

The resulting values of λ and ΔG° are 8349 and −5200 cm^{-1}, respectively. The spectral overlap can therefore be calculated at T = 300 K yielding J = 0.415 eV^{-1}. The resulting electronic rate is k^{ET} = 6.04 × 10^{11} s^{-1}, and the time is τ^{ET} = 1.65 ps.

3.4.2. Excitation Energy Transfer. As the excitation energy transfer process from the excited C_{60} to BODIPY involves localized states, it can be described using the approach based on the individual transition densities of the two fragments, which allows great reduction of the computation requirements.

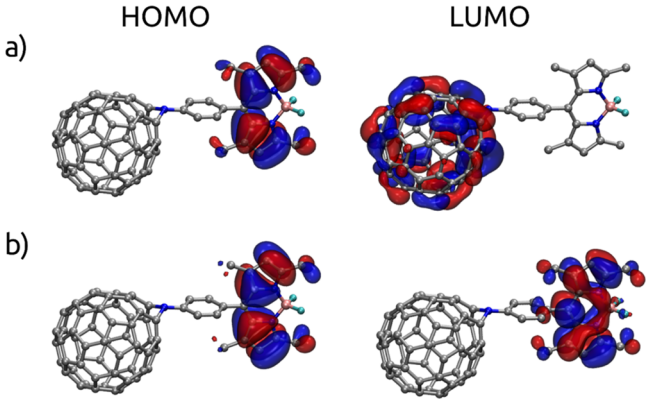

Figure 7. (a) HOMO and LUMO NTOs of the adiabatic state 15, assigned as a BODIPY → C_{60} charge transfer state. (b) HOMO and LUMO NTOs of the adiabatic state 21, which is the first state localized on the BODIPY moiety.

The bright excited states of the fullerene are far higher in energy than the excited state of the BODIPY; however, regardless of the initial excitation, C_{60} relaxes very quickly: the lowest bright state 1^1T_{1u} (400 nm) relaxes in 200 fs, and within 20 ps only the lowest 3 states are populated.[46] These states, however, are far below the excited state of BODIPY. There is no easy way to know which states will be populated shortly after the initial excitation. Therefore, in order to estimate the energy transfer rate, we have only considered the states of C_{60} that are closest in energy to the first state of BODIPY, and with a non-negligible spectral overlap J. The latter has been estimated as described in the Computational Details, after correcting the calculated excitation energies of both fragments to match those resulting from the experimental absorption spectrum.[50]

The states of the C_{60} moiety characterized by a non-negligible spectral overlap with the first state of BODIPY are reported in Table 2. The transfer times obtained range from ∼3 to ∼16 ps. We assume that the nearly degenerate states equilibrate much faster than the EET process. Therefore, the EET rates of nearly degenerate states should be summed. Summing the rate constants of all the C_{60} states in the energy range 2.81−2.98 eV results in an effective rate of 2.86 × 10^{11} s^{-1} and a transfer time of 3.50 ps. On the other hand, considering only state 18, with an energy of 3.45 eV, the rate is slightly higher (3.406 × 10^{11} s^{-1}), resulting in a faster transfer (2.9 ps).

Table 2. Calculated Spectral Overlaps, Electronic Couplings, and EET Rates and Times for the C_{60} States with Significant EET Rate (Shorter than 20 ps)

C_{60} state	overlap J/ eV^{-1}	electronic coupling/ cm^{-1}	EET rate/ s^{-1}	EET time/ ps
11	0.770	30.17	1.028 × 10^{11}	9.7
12	0.904	37.06	1.822 × 10^{11}	5.5
14	1.012	32.05	1.525 × 10^{11}	6.6
17	0.924	21.67	6.367 × 10^{10}	15.7
18	0.836	52.68	3.406 × 10^{11}	2.9

3.4.3. Hole Transfer. In the hole transfer process the hole created after exciting the C_{60} moves to the BODIPY moiety:

$$\text{BODIPY}\ C_{60}\text{*} \rightarrow \text{BODIPY}^{+}\ C_{60}^{-}$$

In this case, the final state is the same as for the ET, but the initial state is localized on the C_{60}. Rates have been computed once again with Marcus theory, where the electronic couplings have been obtained, with the FCD model, between the charge transfer state and the states on fullerene. The reorganization energy was assumed to be the same as in the ET, and the driving force ΔG° has been estimated from the calculated excitation energies of C_{60} in the dyad.

$$\Delta G^\circ_{HT,k} = eE_{ox}(D^+/D) - eE_{red}(A/A^-) + E_{C60,k} + 1/\varepsilon E^{INT}(@D^+A^-)$$

The excitation energies $E_{C60,k}$ were corrected for the method error of 0.7 eV.

In Table 3 the electronic couplings and ΔG° for those states that show a HT rate shorter than 20 ps have been reported.

Table 3. Calculated $-\Delta G^\circ$ and HT Couplings, Rates, and Times for the C_{60} States with Significant HT Rate (up to 20 ps)

C_{60} state	$-\Delta G^\circ/cm^{-1}$	HT coupling/cm^{-1}	HT rate/s^{-1}	HT time/ps
19	−8279	21.1	1.13×10^{11}	8.9
20	−8629	15.9	6.35×10^{10}	15.7
22	−8982	17.3	7.14×10^{10}	14.0
24	−9437	15.3	4.97×10^{10}	20.1
27	−9801	16.5	5.09×10^{10}	19.6
31	−10996	30.9	8.86×10^{10}	11.3

Again, in the EET case, it is not possible to know which states are populated shortly after the initial excitation. To estimate the HT rate, we start from the assumption that the nearly degenerate states will equilibrate much faster than the HT process. In such a case, the observed HT rate should be the sum of the HT rates for the processes that start from these states. Summing the rate constants of all the C_{60} states in the energy range 2.81−2.98 eV leads to an effective rate of 4.33×10^{11} s^{-1} and a transfer time of 2.31 ps.

3.5. Electron Transfer Mechanism at Different Excitation Conditions. The experimental results together with the outcome from the theoretical analysis highlight that, independently of the excitation conditions, the investigated dyad undergoes photoinduced electron transfer, forming the charge separated state BODIPY$^+$ C_{60}^-. Moreover, the experimental and computational results demonstrate that electron transfer from the excited BODIPY toward C_{60} is thermodynamically feasible. Computations of the electron transfer rate, using the Marcus equation, predict a fast electron transfer process, although the computed rate constant is slightly smaller than the experimental one.

When the system is excited in the UV, where most of the excitation energy is absorbed by the C_{60} moiety, the charge separation rate constant increases up to ca. 2 ps. In this case two possible mechanisms could in principle drive the system toward the formation of the final BODIPY$^+$ C_{60}^- state:

(1) The initially excited C_{60}* transfers excitation energy on the BODIPY moiety, and subsequently the BODIPY* C_{60} → BODIPY$^+$ C_{60}^- photoinduced electron transfer takes place.

(2) The electron hole created in the C_{60} HOMO upon electronic excitation moves on the BODIPY moiety with concomitant electron transfer toward the C_{60}.

The theoretical analysis, presented above, evidenced that C_{60} high density of states does not enable exact discrimination between the two alternative mechanisms. In fact the computed rate constants for both the energy and hole transfer processes result of the same order of magnitude of a few picoseconds, making both the alternative processes compatible with the experimental findings. In order to obtain further information on the deactivation pathways occurring upon C_{60} excitation, we measured the transient absorption spectrum of the isolated fullerene in solution. Fullerene excited state dynamics has been extensively studied in the past from both an experimental and theoretical point of view.[44,46−48] The results of our measurements are in line with previous findings; when C_{60} is excited with significant energy excess above its lowest singlet states (lying at ca. 1.9 eV above the ground state), an ultrafast subpicosecond relaxation takes place, eventually populating the S_3 state, which further relaxes on a longer 20−80 ps time scale.[44,46] Since the C_{60} S_3 state lies below the first excited state located on BODIPY, energy transfer from this state toward the BODIPY followed by charge separation appears not favored. On the other hand, energy transfer from an initially excited high energy C_{60}* state toward BODIPY would be competitive with the ultrafast relaxation dynamics of C_{60}*. Although based on several approximations, our theoretical analysis indicates that energy transfer would occur on a time scale of a few picoseconds, which is longer than the measured C_{60} internal conversion time toward its S_3 state. Due to the fast fullerene relaxation, even if the C_{60} → BODIPY energy transfer would occur at rate significantly faster than what we estimated from computations, the process would still be in competition with C_{60} internal conversion, which would greatly reduce its efficiency. Additionally, it is worth noticing that, in the case of a significant yield of C_{60} internal conversion finally populating the fullerene low lying singlets, we would also expect ISC toward the C_{60} triplet to occur, due to its significantly high quantum yield. Our measurements however show that the intensity of the C_{60} triplet signal at 700 nm is minimal (if any is present) on the long time scale upon UV excitation, showing that charge separation is the main deactivation pathway in the dyad at any excitation conditions. Based on these argumentations we suggest that, in the case of selective fullerene excitation, charge separation would proceed through the hole transfer mechanism.

When a less selective 400 nm excitation is used, an intermediate regime is observed: ultrafast electron transfer occurs from the fraction of excited BODIPY*, on the same time scale observed in the case of 475 nm excitation conditions, together with a relatively slower hole transfer from the fraction of excited C_{60}.

Independently of the excitation conditions, the subsequent slower relaxation still deserves some comment. In all the examined cases, the analysis of time-resolved data retrieves two additional time constants, one on the 15−50 ps time scale and the other on a longer nanosecond time scale. The second lifetime is associated with a partial recovery of the BODIPY$^+$ signal, thus to charge recombination. In the case of 475 nm excitation the signal recovers by about 25% on a 13 ps time scale. At the same time a blue shift of the BODIPY$^+$ signal is observed, which could be indicative of radical pair relaxation due to solvent reorganization. In the case of 400 and 266 nm excitation the amount of charge recombination occurring on a ca. 50 ps time scale is on the order of 35−55%. It is worth noticing that although in our system the electron donor and acceptor are directly linked, a significant amount of charge recombination occurs on a nanosecond time scale. The

occurrence of biexponential recombination can be ascribed to the existence of different dyad conformations in solution. The present BODIPY molecule has two methyl groups in the 1,7 positions (see Scheme 1) which partially hinder the rotation around the phenyl group in the *meso* position (position 8, see Scheme 1),[21] however different relative orientations of the BF_2-chelated dipyrromethene core and the *meso*-phenyl substituent can still occur. Geometry optimization of the dyad shows that, in the lowest energy geometry, the BODIPY core and the *meso*-phenyl substituent are perpendicularly oriented, which determines a high degree of orbital localization, and a negligible electron density on the nitrogen connecting the two moieties, in both the HOMO and LUMO of the system. This can be the reason for the observed relatively long charge recombination time. Even in the absence of an extended molecular bridge the amount of electron density delocalization in our system is very limited: the two moieties thus behave as distinct units and not as a single macromolecule, increasing the lifetime of the charge separated state.

4. CONCLUSIONS

Photoinduced electron transfer in the analyzed BODIPY–C_{60} dyad has been shown to occur upon different excitation conditions. The system has been experimentally characterized by means of static and transient absorption spectroscopy and electrochemistry. Spectroelectrochemistry measurements unambiguously identified the spectral signatures due to the formation of the $BODIPY^+$ cation, allowing correct assignment of features in the time-resolved spectra. Based on the analysis of time-resolved data and the results of DFT calculations of electron, energy, and hole transfer rates, we propose a mechanism for charge separation which depends on the excitation conditions. In the case of selective BODIPY excitation, electron transfer would directly proceed from the BODIPY* excited state, while when excitation is on the C_{60} moiety charge separation would preferentially proceed through a hole transfer mechanism. Finally, we have shown that the geometrical arrangement of the two moieties composing the dyad, characterized by an orthogonal orientation of BODIPY and the *meso*-phenyl substituent connecting it to C_{60}, ensures relatively long charge recombination times even in the absence of an extended molecular bridge.

■ ASSOCIATED CONTENT

Supporting Information

The Supporting Information is available free of charge on the ACS Publications website at DOI: 10.1021/acs.jpcc.6b05738.

■ AUTHOR INFORMATION

Corresponding Author

*E-mail: didonato@lens.unifi.it. Tel: +390554962483.

Author Contributions

§A.I. and L.C. have equally contributed to this work.

Notes

The authors declare no competing financial interest.

■ ACKNOWLEDGMENTS

The authors gratefully acknowledge support from the Italian Ministero dell'Istruzione, Università e Ricerca—MIUR program FIRB "Futuro in Ricerca 2010" Grant RBFR10Y5VW to M.D.D. and program FIRB "NANOSOLAR" and Program FIRB "Approcci nanotecnologici per la teragnostica dei tumori" Grant RBAP11ETKA_002 to S. Cicchi. L.C., S. Caprasecca, and B.M. acknowledge the European Research Council (ERC) for financial support in the framework of the Starting Grant (Enlight-277755). M.D.D. wishes to acknowledge the contribution of "Ente Cassa di Risparmio di Firenze". Laserlab Europe Contract No. 654148 and University of Bologna are also gratefully acknowledged.

■ REFERENCES

(1) Fukuzumi, S.; Ohkubo, K. Assemblies of Artificial Photosynthetic Reaction Centres. *J. Mater. Chem.* **2012**, *22*, 4575–4587.

(2) Gust, D.; Moore, T. A.; Moore, A. L. Solar Fuels via Artificial Photosynthesis. *Acc. Chem. Res.* **2009**, *42*, 1890–1898.

(3) Wasielewski, M. R. Self-Assembly Strategies for Integrating Light Harvesting and Charge Separation in Artificial Photosynthetic Systems. *Acc. Chem. Res.* **2009**, *42*, 1910–1921.

(4) Hasobe, T. Supramolecular Nanoarchitectures for Light Energy Conversion. *Phys. Chem. Chem. Phys.* **2010**, *12*, 44–57.

(5) Balzani, V.; Credi, A.; Venturi, M. Photochemical Conversion of Solar Energy. *ChemSusChem* **2008**, *1*, 26–58.

(6) Barber, J. Photosynthetic Energy Conversion: Natural and Artificial. *Chem. Soc. Rev.* **2009**, *38*, 185–196.

(7) Scholes, G. D.; Fleming, G. R.; Olaya-Castro, A.; van Grondelle, R. Lessons from Nature about Solar Light Harvesting. *Nat. Chem.* **2011**, *3*, 763–744.

(8) El-Khouly, M. E.; Fukuzumi, S.; D'Souza, F. Photosynthetic Antenna–Reaction Center Mimicry by Using Boron Dipyrromethene Sensitizers. *ChemPhysChem* **2014**, *15*, 30–47.

(9) Imahori, H.; Tamaki, K.; Guldi, D. M.; Luo, C.; Fujitsuka, M.; Ito, O.; Sakata, Y.; Fukuzumi, S. Modulating Charge Separation and Charge Recombination Dynamics in Porphyrin-Fullerene Linked Dyads and Triads: Marcus-Normal versus Inverted Region. *J. Am. Chem. Soc.* **2001**, *123*, 2607–2617.

(10) Kamimura, T.; Ohkubo, K.; Kawashima, Y.; Ozako, S.; Sakaguchi, K.-i.; Fukuzumi, S.; Tani, F. Long-Lived Photoinduced Charge Separation in Inclusion Complexes Composed of a Phenothiazine-Bridged Cyclic Porphyrin Dimer and Fullerenes. *J. Phys. Chem. C* **2015**, *119*, 25634–25650.

(11) Pla, S.; Niemi, M.; Martin-Gomis, L.; Fernandez-Lazaro, F.; Lemmetyinen, H.; Tkachenko, N. V.; Sastre-Santos, A. Charge Separation and Charge Recombination Photophysical Studies in a Series of Perylene-C_{60} Linear and Cyclic Dyads. *Phys. Chem. Chem. Phys.* **2016**, *18*, 3598–3605.

(12) Trukhina, O.; Rudolf, M.; Bottari, G.; Akasaka, T.; Echegoyen, L.; Torres, T.; Guldi, D. M. Bidirectional Electron Transfer Capability in Phthalocyanine-$Sc_3N@I_h$-C_{80} Complexes. *J. Am. Chem. Soc.* **2015**, *137*, 12914–12922.

(13) Virkki, K.; Demir, S.; Lemmetyinen, H.; Tkachenko, N. V. Photoinduced Electron Transfer in CdSe/ZnS Quantum Dot-Fullerene Hybrids. *J. Phys. Chem. C* **2015**, *119*, 17561–17572.

(14) Shi, W.-J.; El-Khouly, M. E.; Ohkubo, K.; Fukuzumi, S.; Ng, D. K. P. Photosynthetic Antenna-Reaction Center Mimicry with a Covalently Linked Monostyryl Boron-Dipyrromethene–Aza-Boron-Dipyrromethene–C_{60} Triad. *Chem. - Eur. J.* **2013**, *19*, 11332–11341.

(15) Bai, D.; Benniston, A. C.; Hagon, J.; Lemmetyinen, H.; Tkachenko, N. V.; Harrington, R. W. Tuning the Forster Overlap Integral: Energy Transfer over 20 Angstroms from a Pyrene-Based Donor to Borondipyrromethene (Bodipy). *Phys. Chem. Chem. Phys.* **2013**, *15*, 9854–9861.

(16) Sabatini, R. P.; McCormick, T. M.; Lazarides, T.; Wilson, K. C.; Eisenberg, R.; McCamant, D. W. Intersystem Crossing in Halogenated Bodipy Chromophores Used for Solar Hydrogen Production. *J. Phys. Chem. Lett.* **2011**, *2*, 223–227.

(17) D'Souza, F.; Smith, P. M.; Zandler, M. E.; McCarty, A. L.; Itou, M.; Araki, Y.; Ito, O. Energy Transfer Followed by Electron Transfer

in a Supramolecular Triad Composed of Boron Dipyrrin, Zinc Porphyrin, and Fullerene: A Model for the Photosynthetic Antenna-Reaction Center Complex. *J. Am. Chem. Soc.* **2004**, *126*, 7898−7907.
(18) Guo, S.; Ma, L.; Zhao, J.; Kucukoz, B.; Karatay, A.; Hayvali, M.; Yaglioglu, H. G.; Elmali, A. BODIPY Triads Triplet Photosensitizers Enhanced with Intramolecular Resonance Energy Transfer (RET): Broadband Visible Light Absorption and Application in Photooxidation. *Chem. Sci.* **2014**, *5*, 489−500.
(19) Bandi, V.; Gobeze, H. B.; D'Souza, F. Ultrafast Photoinduced Electron Transfer and Charge Stabilization in Donor−Acceptor Dyads Capable of Harvesting Near-Infrared Light. *Chem. - Eur. J.* **2015**, *21*, 11483−11494.
(20) Di Donato, M.; Iagatti, A.; Lapini, A.; Foggi, P.; Cicchi, S.; Lascialfari, L.; Fedeli, S.; Caprasecca, S.; Mennucci, B. Combined Experimental and Theoretical Study of Efficient and Ultrafast Energy Transfer in a Molecular Dyad. *J. Phys. Chem. C* **2014**, *118*, 23476−23486.
(21) Loudet, A.; Burgess, K. BODIPY Dyes and Their Derivatives: Syntheses and Spectroscopic Properties. *Chem. Rev.* **2007**, *107*, 4891−4932.
(22) Fedeli, S.; Brandi, A.; Venturini, L.; Chiarugi, P.; Giannoni, E.; Paoli, P.; Corti, D.; Giambastiani, G.; Tuci, G.; Cicchi, S. The "Click-on-Tube" Approach for the Production of Efficient Drug Carriers Based on Oxidized Multi-Walled Carbon Nanotubes. *J. Mater. Chem. B* **2016**, *4*, 3823−3831.
(23) Fedeli, S.; Paoli, P.; Brandi, A.; Venturini, L.; Giambastiani, G.; Tuci, G.; Cicchi, S. Azido-Substituted BODIPY Dyes for the Production of Fluorescent Carbon Nanotubes. *Chem. - Eur. J.* **2015**, *21*, 15349−15353.
(24) Prato, M.; Li, Q. C.; Wudl, F.; Lucchini, V. Addition of Azides to Fullerene C60: Synthesis of Azafulleroids. *J. Am. Chem. Soc.* **1993**, *115*, 1148−1150.
(25) Wu, R.; Lu, X.; Zhang, Y.; Zhang, J.; Xiong, W.; Zhu, S. Addition Reactions of Fluoroalkanesulfonyl Azides to [60] Fullerene Under Thermal or Microwave Irradiation Condition. *Tetrahedron* **2008**, *64*, 10694−10698.
(26) Strom, T. A.; Barron, A. R. A Simple Quick Route to Fullerene Amino Acid Derivatives. *Chem. Commun.* **2010**, *46*, 4764−4766.
(27) Gentili, P. L.; Mugnai, M.; Bussotti, L.; Righini, R.; Foggi, P.; Cicchi, S.; Ghini, G.; Viviani, S.; Brandi, A. The Ultrafast Energy Transfer Process in Naphtol-nitrobenzofurazan Bichromophoric Molecular Systems: A Study by Femtosecond UV-vis Pump-Probe Spectroscopy. *J. Photochem. Photobiol., A* **2007**, *187*, 209−221.
(28) Bayanov, I. M.; Danielius, R.; Heinz, P.; Seilmeier, A. Intense Subpicosecond Pulses Tunable Between 4 and 20 μm Generated by an All-Solid-State Laser System. *Opt. Commun.* **1994**, *113*, 99−104.
(29) Danielius, R.; Piskarskas, A.; Di Trapani, P.; Andreoni, A.; Solcia, C.; Foggi, P. Visible pulses of 100 fs and 100 μJ from an Upconverted Parametric Generator. *Appl. Opt.* **1996**, *35*, 5336−5339.
(30) Bruno, C.; Doubitski, I.; Marcaccio, M.; Paolucci, F.; Paolucci, D.; Zaopo, A. Electrochemical Generation of C_{60}^{2+} and C_{60}^{3+}. *J. Am. Chem. Soc.* **2003**, *125*, 15738−15739.
(31) Marcaccio, M.; Paolucci, F.; Paradisi, C.; Carano, M.; Roffia, S.; Fontanesi, C.; Yellowlees, L. J.; Serroni, S.; Campagna, S.; Balzani, V. Electrochemistry and Spectroelectrochemistry of Ruthenium(II)-Bipyridine Building Blocks. Different Behaviour of the 2,3- and 2,5-bis(2-pyridyl)pyrazine Bridging Ligands. *J. Electroanal. Chem.* **2002**, *532*, 99−112.
(32) Amatore, C.; Lefrou, C. New Concept for a Potentiostat for On-Line Ohmic Drop Compensation in Cyclic Voltammetry Above 300 kV. *J. Electroanal. Chem.* **1992**, *324*, 33−58.
(33) Mottier, L. *Antigona*; University of Bologna: Bologna, Italy, 1999.
(34) Bruno, C.; Paolucci, F.; Marcaccio, M.; Benassi, R.; Fontanesi, C.; Mucci, A.; Parenti, F.; Preti, L.; Schenetti, L.; Vanossi, D. Experimental and Theoretical Study of the p- and n-Doped States of Alkylsulfanyl Octithiophenes. *J. Phys. Chem. B* **2010**, *114*, 8585−8592.
(35) Lee, S.-M.; Marcaccio, M.; McCleverty, J. A.; Ward, M. D. Dinuclear Complexes Containing Ferrocenyl and Oxomolybdenum-(V) Groups Linked by Conjugated Bridges: A New Class of Electrochromic Near-Infrared Dye. *Chem. Mater.* **1998**, *10*, 3272−3274.
(36) Tomasi, J.; Mennucci, B.; Cammi, R. Quantum Mechanical Continuum Solvation Models. *Chem. Rev.* **2005**, *105*, 2999−3094.
(37) Iozzi, M. F.; Mennucci, B.; Tomasi, J.; Cammi, R. Excitation Energy Transfer (EET) between molecules in condensed matter: A novel application of the polarizable Continuum Model (PCM). *J. Chem. Phys.* **2004**, *120*, 7029−7040.
(38) Voityuk, A. A.; Rösch, N. Fragment Charge Difference Method for Estimating Donor-Acceptor Electronic Coupling: Application to DNA-Stacks. *J. Chem. Phys.* **2002**, *117*, 5607−5616.
(39) Lee, S.-J.; Chen, H.-C.; You, Z.-Q.; Liu, K.-L.; Chow, T. J.; Chen, I. C.; Hsu, C.-P. Theoretical Characterization of Photoinduced Electron Transfer in Rigidly Linked Donor-Acceptor Molecules: the Fragment Charge Difference and the Generalized Mulliken-Hush Schemes. *Mol. Phys.* **2010**, *108*, 2775−2789.
(40) Vaissier, V.; Barnes, P.; Kirkpatrick, J.; Nelson, J. Influence of Polar Medium on the Reorganization Energy of Charge Transfer Between Dyes in a Dye Sensitized Film. *Phys. Chem. Chem. Phys.* **2013**, *15*, 4804−4814.
(41) Rehm, D.; Weller, A. Kinetics of Fluorescence Quenching by Electron and H-Atom Transfer. *Isr. J. Chem.* **1970**, *8*, 259−271.
(42) Paolucci, F.; Marcaccio, M.; Roffia, S.; Orlandi, G.; Zerbetto, F.; Prato, M.; Maggini, M.; Scorrano, G. Electrochemical Monitoring of Valence Bond Isomers Interconversion in Bipyridyl-C61 Anions. *J. Am. Chem. Soc.* **1995**, *117*, 6572−6580.
(43) Dubois, D.; Kadish, K. M.; Flanagan, S.; Haufler, R. E.; Chibante, L. P. F.; Wilson, L. J. Spectroelectrochemical Study of the C_{60} and C_{70} Fullerenes and their Mono-, di-, tri- and Tetraanions. *J. Am. Chem. Soc.* **1991**, *113*, 4364−4366.
(44) Sassara, A.; Zerza, G.; Ciulin, V.; Portella-Oberli, M. T.; Ganière, J. D.; Deveaud, B.; Chergui, M. Picosecond and Femtosecond Studies of the Energy Redistribution in Matrix-Isolated C_{60} Molecules. *J. Lumin.* **1999**, *83*−*84*, 29−32.
(45) Sension, R. J.; Phillips, C. M.; Szarka, A. Z.; Romanow, W. J.; McGhie, A. R.; McCauley, J. P.; Smith, A. B.; Hochstrasser, R. M. Transient Absorption Studies of Carbon (C_{60}) in Solution. *J. Phys. Chem.* **1991**, *95*, 6075−6078.
(46) Stepanov, A. G.; Portella-Oberli, M. T.; Sassara, A.; Chergui, M. Ultrafast Intramolecular Relaxation of C_{60}. *Chem. Phys. Lett.* **2002**, *358*, 516−522.
(47) Palit, D. K.; Sapre, A. V.; Mittal, J. P.; Rao, C. N. R. Photophysical Properties of the Fullerenes, C_{60} and C_{70}. *Chem. Phys. Lett.* **1992**, *195*, 1−6.
(48) Orlandi, G.; Negri, F. Electronic States and Transitions in C_{60} and C_{70} Fullerenes. *Photochem. Photobiol. Sci.* **2002**, *1*, 289−308.
(49) Dreuw, A.; Head-Gordon, M. Single-Reference ab Initio Methods for the Calculation of Excited States of Large Molecules. *Chem. Rev.* **2005**, *105*, 4009−4037.
(50) Leach, S.; Vervloet, M.; Desprès, A.; Bréheret, E.; Hare, J. P.; John Dennis, T.; Kroto, H. W.; Taylor, R.; Walton, D. R. M. Electronic Spectra and Transitions of the Fullerene C_{60}. *Chem. Phys.* **1992**, *160*, 451−466.